Comparison of Aqueous and Non-Aqueous Binder Materials and the Mixing Ratios for Zn-MnO$_2$ Batteries with Mildly Acidic Aqueous Electrolytes

Oliver Fitz[1,*], Stefan Ingenhoven[1], Christian Bischoff[1], Harald Gentischer[1], Kai Peter Birke[2], Dragos Saracsan[3] and Daniel Biro[4]

S1. Brief literature research on binder materials, solvents, electrode composition ratios and current collectors

Table S1: Brief literature research on binder materials, solvents, mixing ratios and current collectors. This literature search was carried out as an example and does not claim to be complete.

source	electrode production process	binder polymer (BP) (solvent)	composition AM-CB-BP	comment[1]	electrochemical performance
[1]	doctor blade coating	PVDF (NMP), CMC (water), Na-alginate (water), CMC (water)+PVA	70-20-10	current collector: Titanium	280 mAh.g^{-1} @ 100 mA.g^{-1}
[2]	doctor blade coating	PVDF(NMP)	70-20-10	current collector: Steel mesh	- / investigations on negative anode
[3]	doctor blade coating	PVDF(NMP)	60-30-10	current collector: Carbon Paper Electrolyte: Zn(TFSI)$_2$ + MnSO$_4$ (aq.)	212 mAh @ "5C"
[4]	doctor blade coating	PVDF(NMP)	75-15-10	current collector: Steel mesh	218 mAh.g^{-1} @ 123 mA.g^{-1}
[5]	pasting/smearing	PVDF (Solvent not specified)	80-10-10	current collector: Ti mesh	270 mAh.g^{-1} @ 30 mA.g^{-1}
[6]	doctor blade coating	PVDF (Solvent not specified)	70-20-10	current collector: Titanium	270 mAh.g^{-1} @ "1C"
[7]	doctor blade coating	LA133 (water)+ CMC (water) (8:2)	70-20-8(LA133)-2(CMC)	active material: MnO2/CNT nanocomposite,	665 mAh.g^{-1} @ 100 mA.g^{-1}

---

[1] Electrolytes contain ZnSO$_4$ or MnSO$_4$, if not stated otherwise.

				current collector: Steel foil	
[8]	doctor blade coating	LA133 (water)	70-20-10	current collector: Steel foil	80 mAh.g^{-1} @ 100 mA.g^{-1}
[9]	doctor blade coating	PVDF (NMP)	80-11(2% Graphite, 9% carbon Black)-9	current collector: Carbon Paper	233 mAh.g^{-1} @ 30 mA.g^{-1}
[10]	doctor blade coating	PVDF (NMP)	85-10-5	current collector: Steel foil; Electrolyte: $Zn(CF_3SO_3)_2$ (aq.)	230 mAh.g^{-1} @ 200 mA.g^{-1}
[11]	doctor blade coating	LA133 (water)	70-20-10	current collector: Steel foil	139 mAh.g^{-1} @ 100 mA.g^{-1}
[12]	doctor blade coating	PVDF (NMP)	70-20-10	current collector: Carbon sheets	300 mAh.g^{-1} @ 103 mA.g^{-1}
[13]	doctor blade coating	CMC (water)/SBR (water)	80-10-10	MnO2-nanorods	312 mAh.g^{-1} @ 33 mA.g^{-1}
[14]	pasting	PTFE	60-30-10	Pressed Paste current collector: Steel Gauze Circle	103 mAh.g^{-1} @ 300 mA.g^{-1}
[15]	doctor blade coating	PTFE	80-10-10	active material: PANI intercalated MnO2 current collector: Ti-grid	280 mAh.g^{-1} @ 200 mA.g^{-1}
[16]	electrodeposition EMD	-	-	carbon cloth	Different denotation used
[17]	pasting	PVDF	70-20-10	stainless steel wire mesh	300 mAh.g^{-1} @ 100 mA.g^{-1}
[18]	electrodeposition EMD	-	-	carbon fibre paper	290 mAh.g^{-1} @ 90 mA.g^{-1}
[19]	doctor blade coating	PVDF (NMP)	70-20-10	Stainless steel foil (30 µm), first application of conductive CB+BP layer	187 mAh.g^{-1} @ 100 mA.g^{-1}
[20]	doctor blade coating	PVDF (NMP)	70-10-20	Stainless steel foil (25 µm)	200 mAh.g^{-1} @ 42 mA.g^{-1}
[21]	doctor blade coating	PVDF (NMP)	70-10-20	Stainless steel foil (25 µm)	167 mAh.g^{-1} @ 42 mA.g^{-1}
[22]	tableting	PTFE	70-20-10	Active material: α-MnO2 Nanowires	362,6 mAh.g^{-1} @ 300 mA.g^{-1}

				No current collector	
[23]	Pressing	TAB	70-20-10	Stainless steel mesh	250 mAh.g^{-1} @ 0.5 mA.cm^{-2}
[24]	Pressing	TAB	70-20-10	Stainless steel mesh	252 mAh.g^{-1} @ 83 mA.g^{-1}
[25]	doctor blade coating	PVDF (NMP)	80-10-10	Carbon coated aluminium foil Electrolyte: 0,5 Zn(TFSI)$_2$ in Acrylonitrile	110 mAh.g^{-1} @ 12.3 mA.g^{-1}

S2. Experimental cell setup using EL Cell® ECC aqu

copper coin, ø 18 mm

zinc foil (d=25 µm), ø 16 mm

separator, ø 18 mm

pos. electrode @ stainless steel foil (d=25 µm), ø 16 mm

stainless steel coin, ø 18 mm
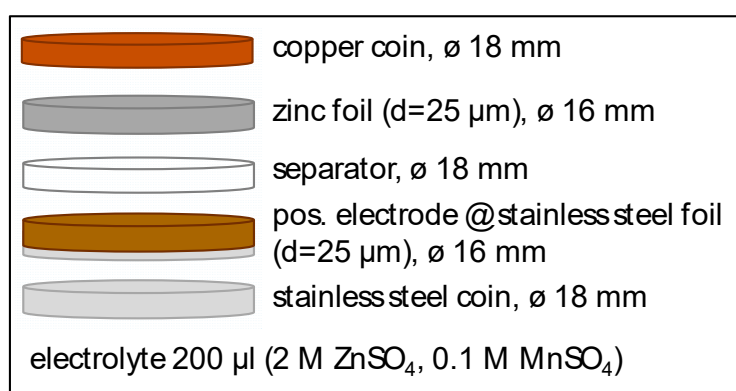
electrolyte 200 µl (2 M ZnSO$_4$, 0.1 M MnSO$_4$)

Figure S1: Overview of the experimental cell setup inside the EL-Cell® ECC aqu.

S3. Rate Capability Test (RCT): Test plan procedure

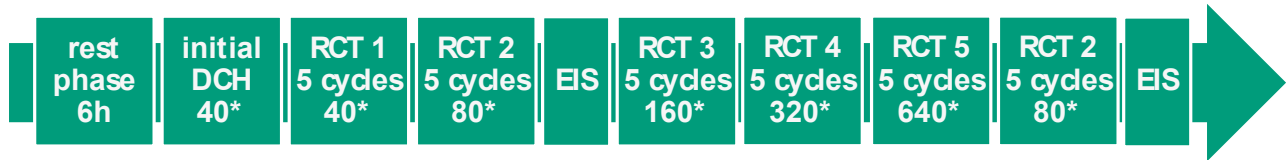| rest phase 6h | initial DCH 40* | RCT 1 5 cycles 40* | RCT 2 5 cycles 80* | EIS | RCT 3 5 cycles 160* | RCT 4 5 cycles 320* | RCT 5 5 cycles 640* | RCT 2 5 cycles 80* | EIS |

Figure S2: Graphical overview of the test plan procedure for the rate capability test of the herein tested cells.

Table S2: Detailed Overview of the test plan procedure for the RCT.

| Cycle		Mass specific current rate $i_{Cycling}$ / mA.g$_{AM}^{-1}$	Number of loops	Comment
	Rest		-	6 hours
1	Discharge	40	-	Initial discharge
2 – 6	Charge Discharge	40	5	
7 – 11	Charge Discharge	80	5	
	PEIS			PEIS-measurements at 1.7 V, 1.25 V and 0.8 V; 2 hours rest before each measurement
12 – 16	Charge Discharge	160	5	
17 – 21	Charge Discharge	320	5	
22 – 26	Charge Discharge	640	5	
27 – 31	Charge Discharge	80	5	
	PEIS			PEIS-measurements at 1.7 V, 1.25 V and 0.8 V; 2 hours rest before each measurement

S4. Mechanical Stress Test (MST): Experimental setup
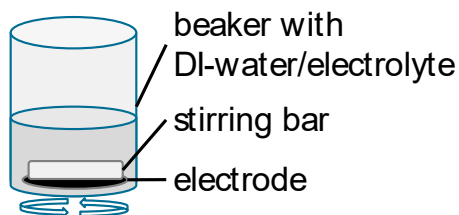
Figure S3: Experimental setup of the mechanical stress test with a magnetic stirring bar in a PP beaker (20 ml, ø31x48 mm) filled with ~ 10 ml of liquid.

S5. Derivation: overpotentials by increasing ohmic resistance in energy plot
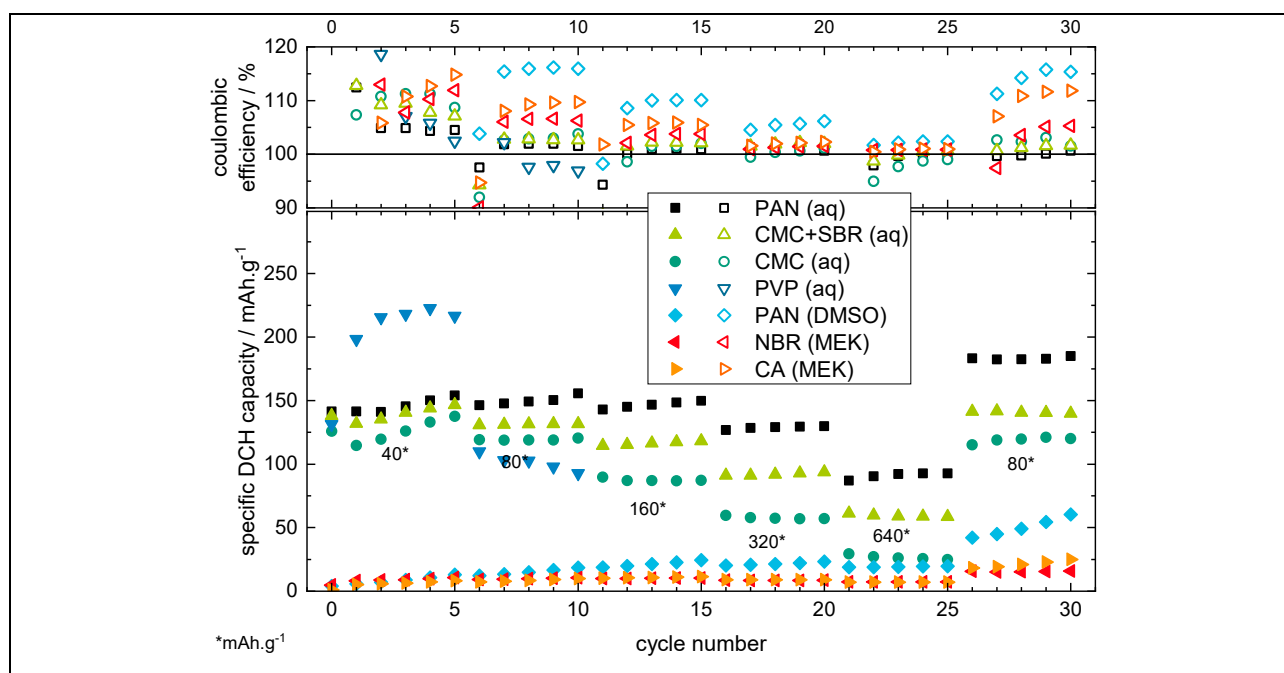
$$E = C * U \qquad (1)$$

$$U = R * I \qquad (2)$$

$$E = C * R * I \qquad (3)$$

with $I = const.$ (determined by constant current cycling rate of CC-step)

Here, E means energy, C means electric charge (capacity), U means voltage, R means ohmic resistance, I means current.
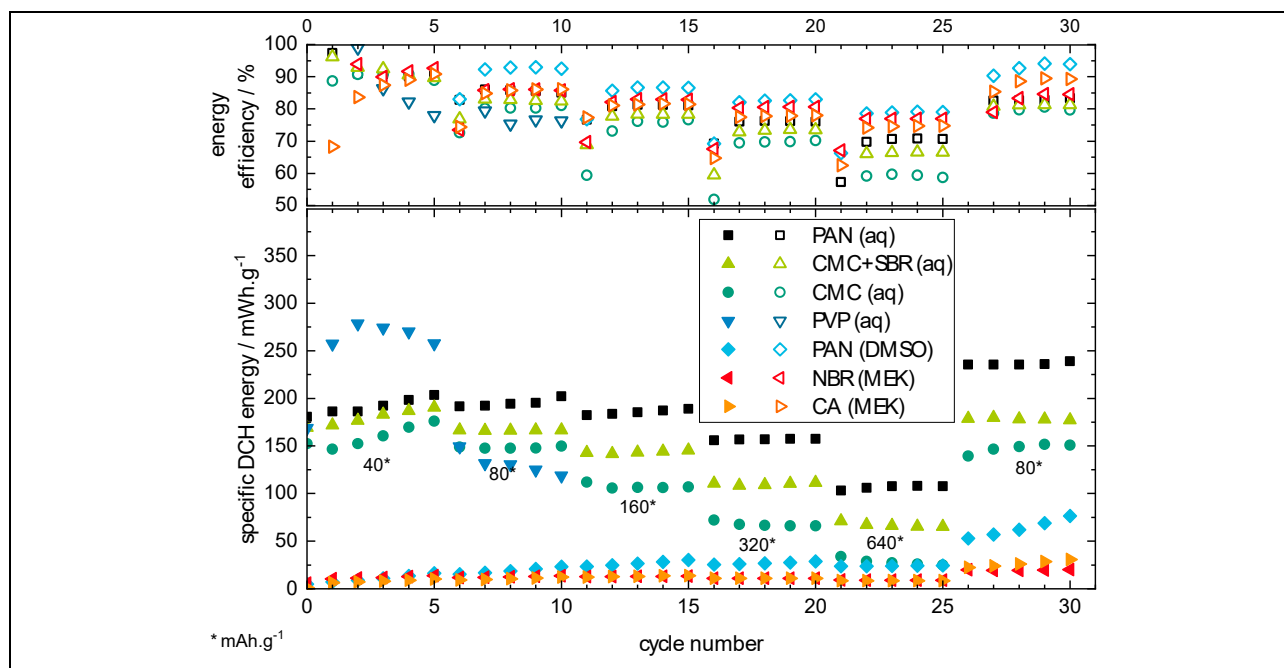
S6. Binder variation: PVP results

Figure S4: RCT results including the PVP (aq) binder polymer, which is not finishing the RCT due to stability issues of the electrode coating (s. MST).
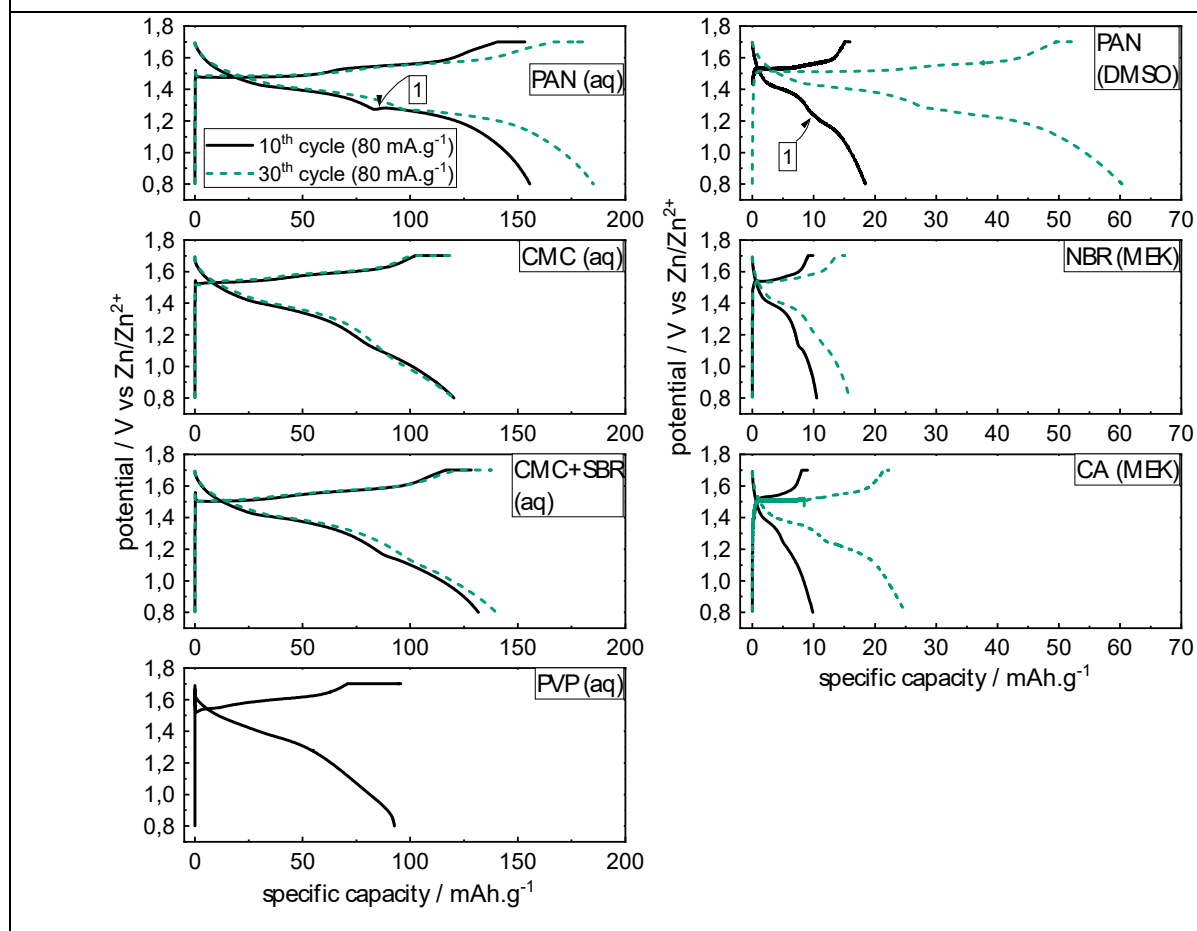

Figure S5: Potential curves including the PVP binder, which was not able to finish the RCT.

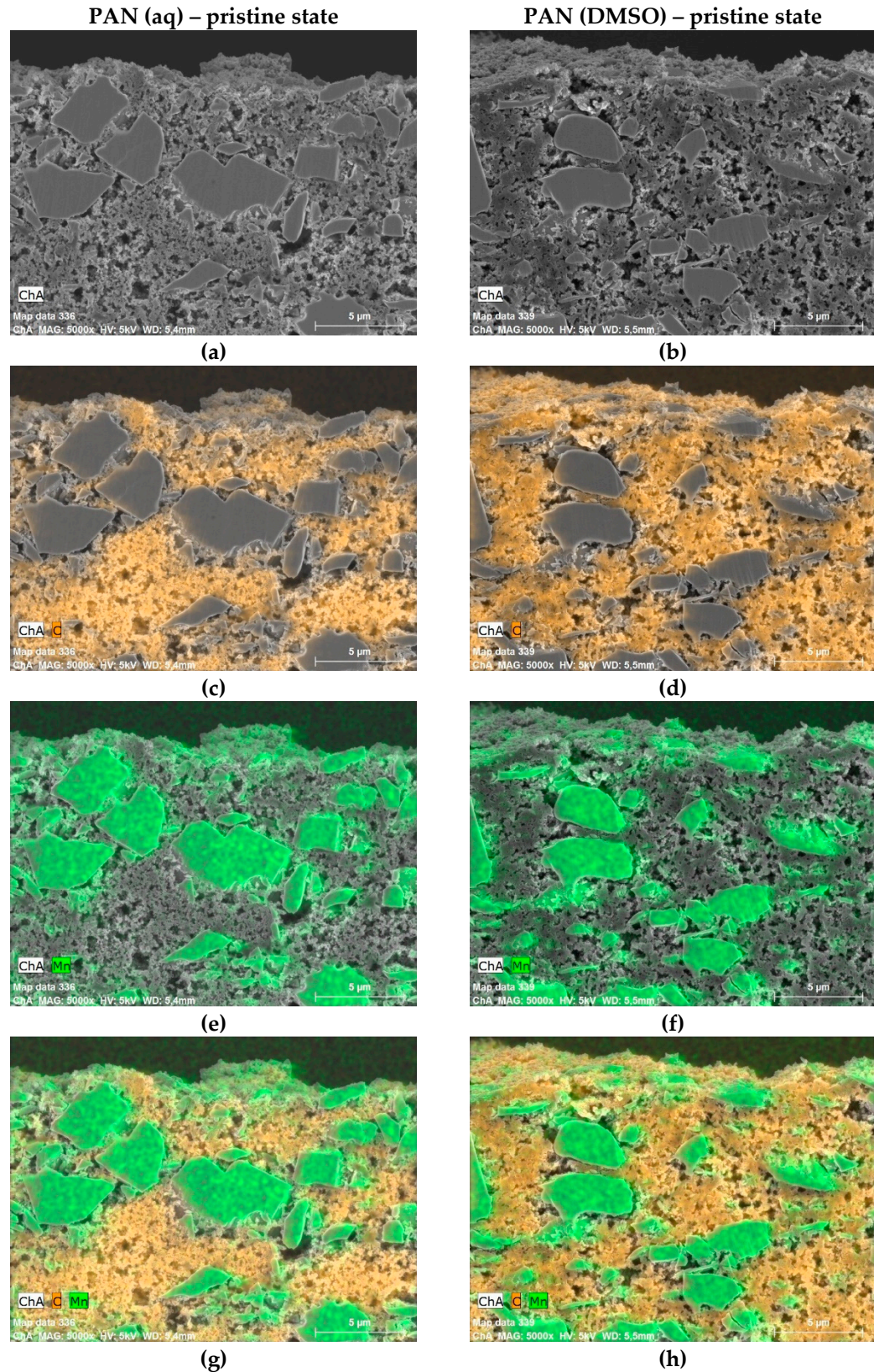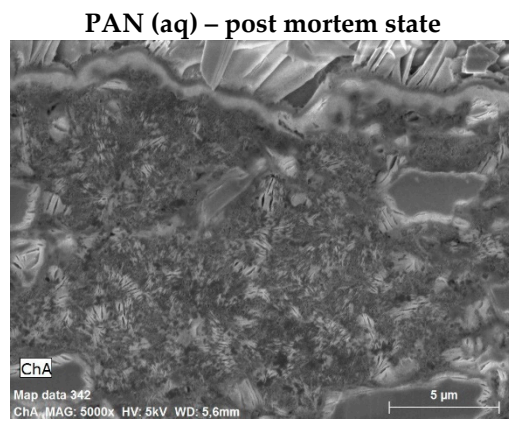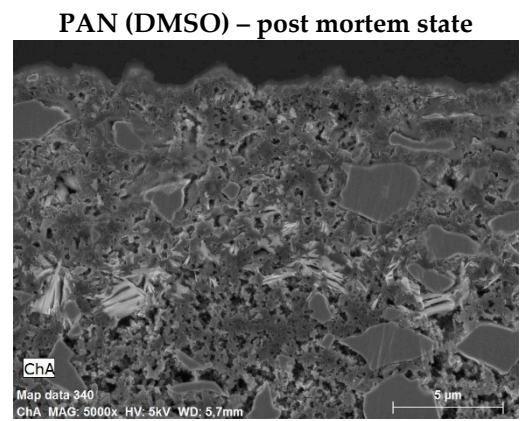# S7. SEM+EDX: PAN (aq) vs. PAN (DMSO), pristine vs post mortem state

PAN (aq) – pristine state | **PAN (DMSO) – pristine state**
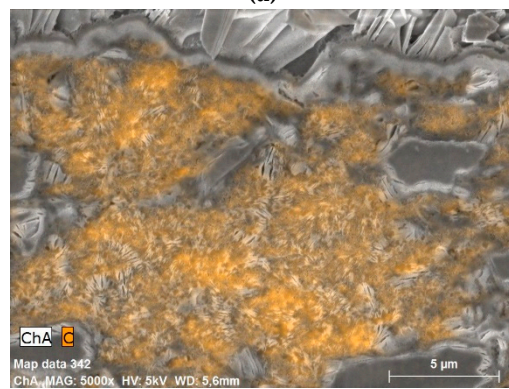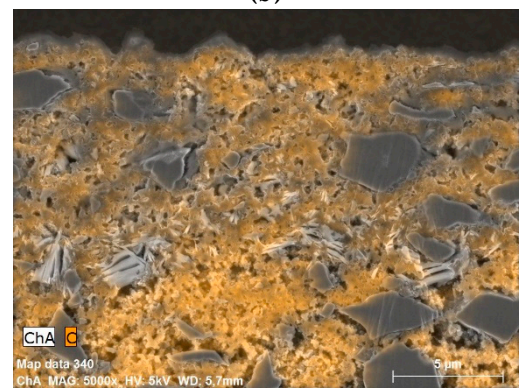

(a)

(b)

(c)

(d)

(e)

(f)

(g)

(h)

Figure S6: Comparison of the PAN (aq) and the PAN (DMSO) coating in pristine state. MnO_2 particles are coloured green, carbon black is coloured orange.

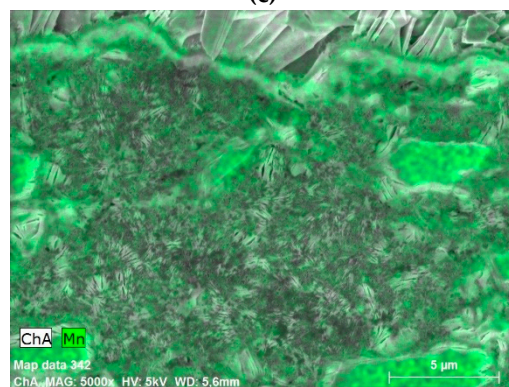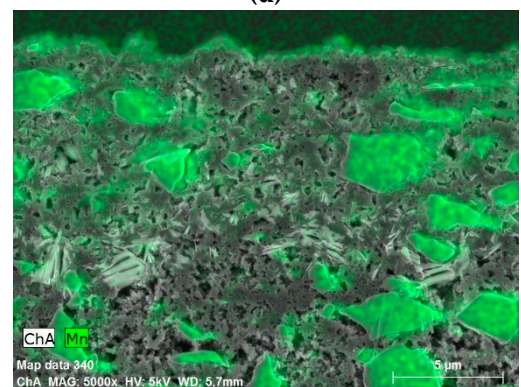**PAN (aq) – post mortem state**   **PAN (DMSO) – post mortem state**

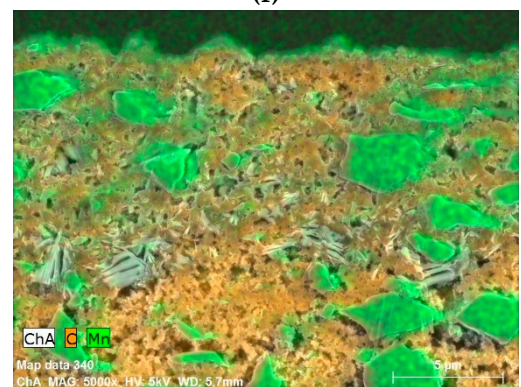*Figure S7: Comparison of the PAN (aq) and the PAN (DMSO) coating in post mortem state. MnO$_2$ particles are coloured green, carbon black is coloured orange.*

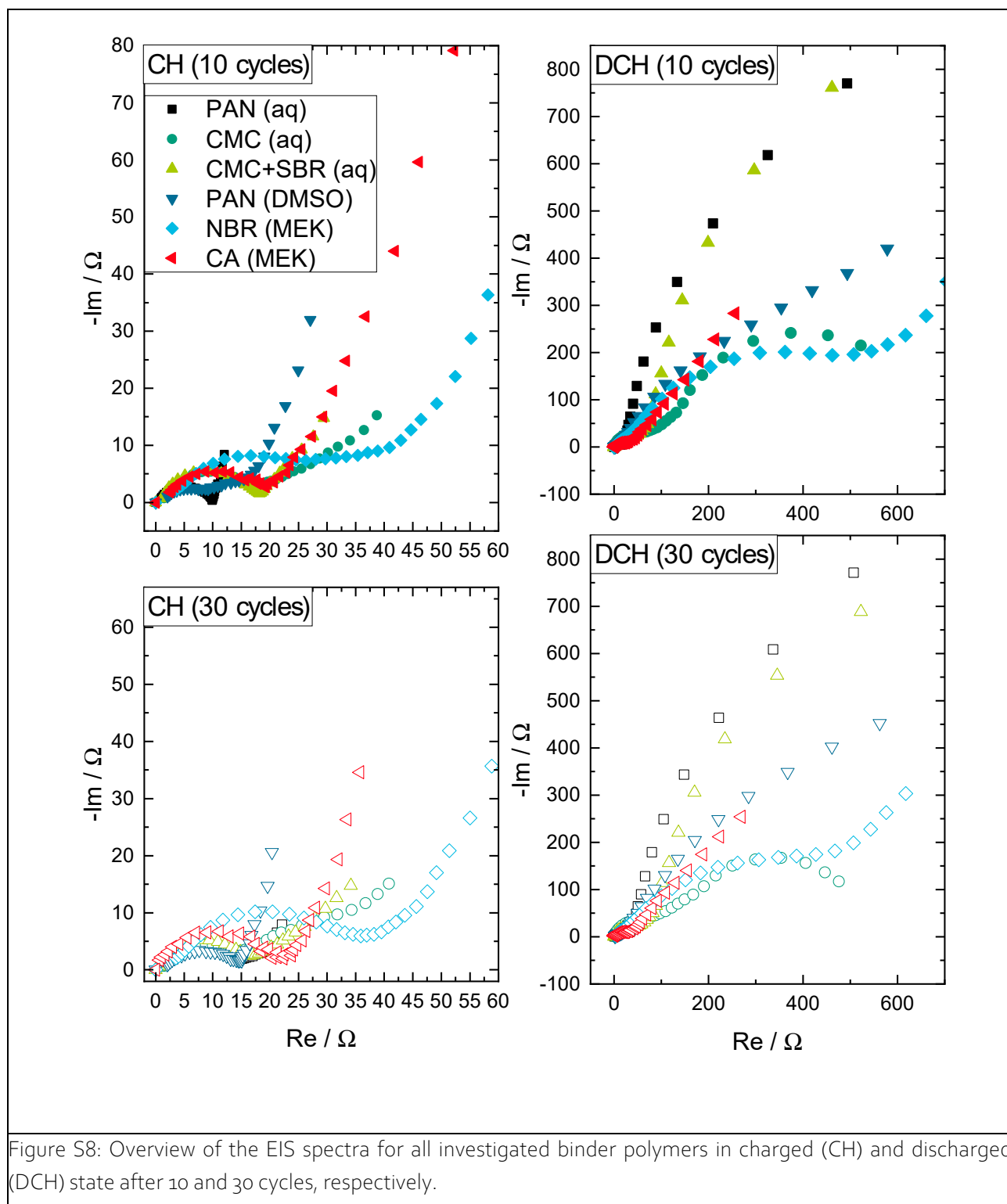## S8. Binder variation: EIS results

Figure S8: Overview of the EIS spectra for all investigated binder polymers in charged (CH) and discharged (DCH) state after 10 and 30 cycles, respectively.
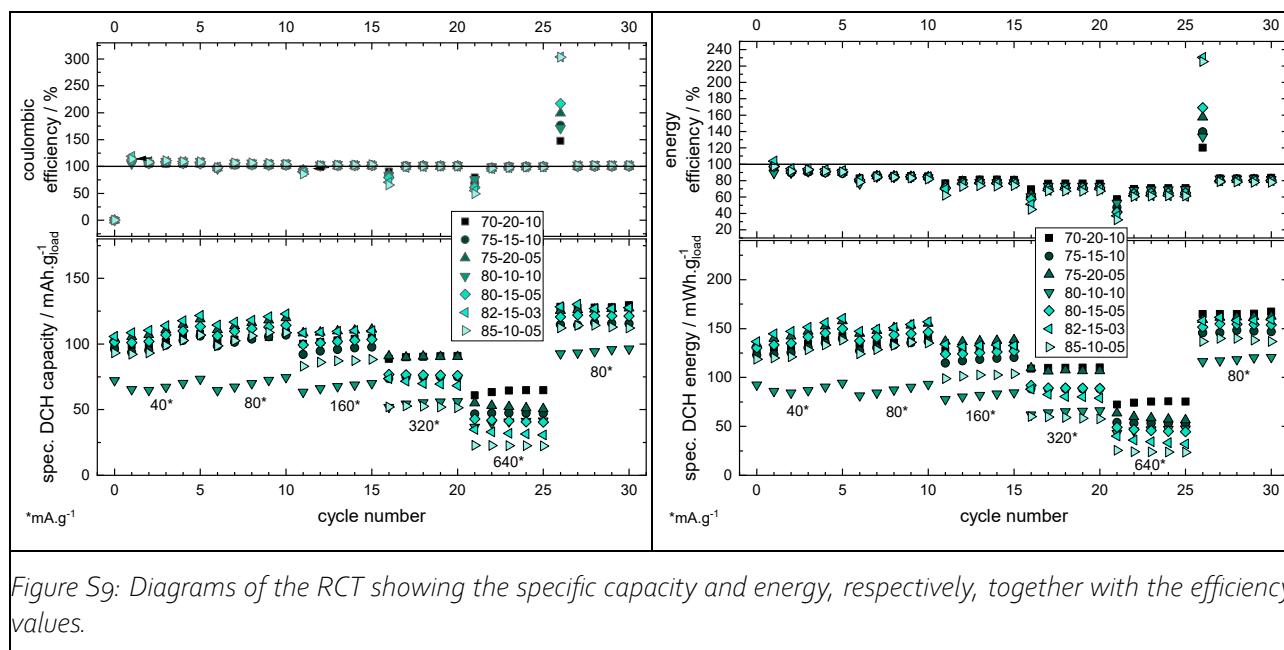
S9. Mixing ratio comparison: efficiency details

Figure S9: Diagrams of the RCT showing the specific capacity and energy, respectively, together with the efficiency values.

Compared to the presentation of the results in the paper, the y-axis of the efficiency values shows all the efficiency results of the cells, respectively, including the deviating values after a change of the current rate. This deviation can be related to a reduced discharge capacity during the first discharge step of each of the current rates (increasing overpotential for increasing current rate) in comparison to the related charge step, in consequence of the major influence of MnO_2 deposition/dissolution mechanism in ARZIBs. Noticeably, this behaviour happens vice versa for the last current rate change from 640 to 80 mAh.g^{-1}, due to an additional discharge capacity in consequence of a reduction of the overpotential for decreasing current rates.

S10. SEM+EDX for selected coatings

70/20/10 – pristine state

Figure S10: SEM+EDX images of the coating with aqueous LA133 (PAN-based) binder with the mixing ration 70/20/10 (AM/CB/BP, wt%) in pristine state. The electrode thickness is ~40 μm.
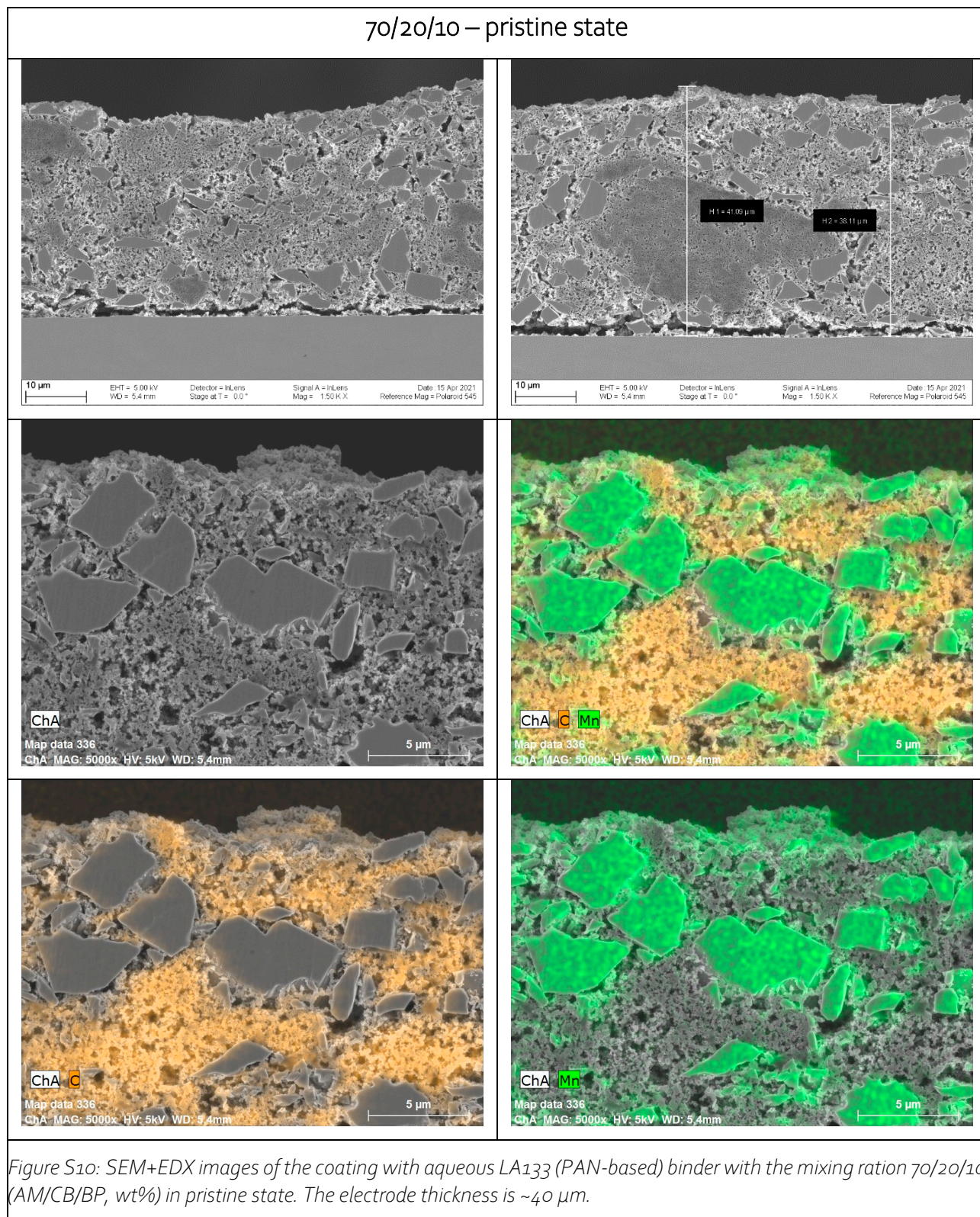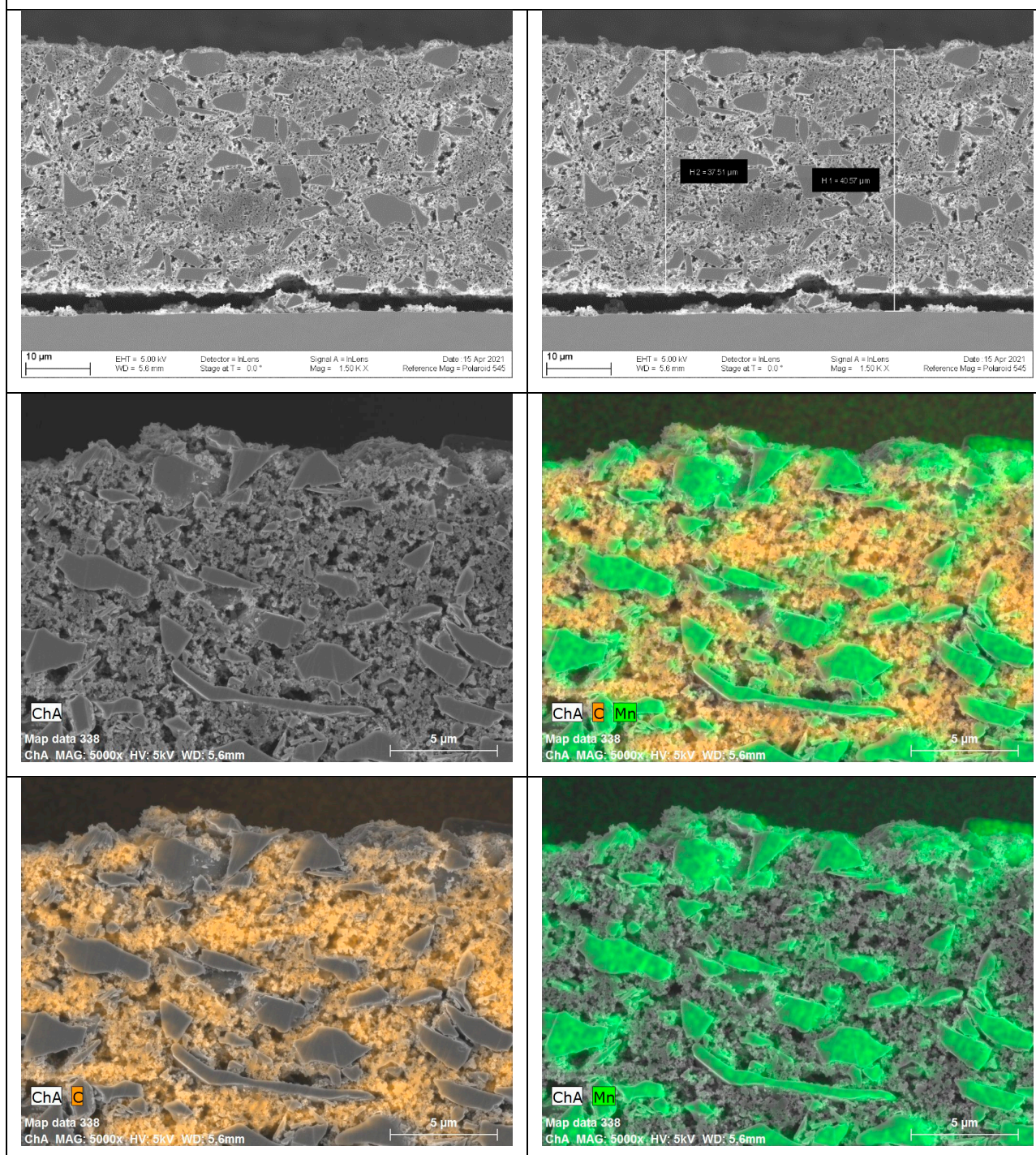
80/15/05 – pristine state

Figure S11: SEM+EDX images of the coating with aqueous LA133 (PAN-based) binder with the mixing ration of 80/15/05 (AM/CB/BP, wt%) in pristine state. The electrode thickness is ~40 µm. (green coloured = MnO₂ particles, orange coloured = carbon black (CB)).

70/20/10 – pristine state   **80/15/05 – pristine state**

(a)   (b)

(c)   (d)

(e)   (f)

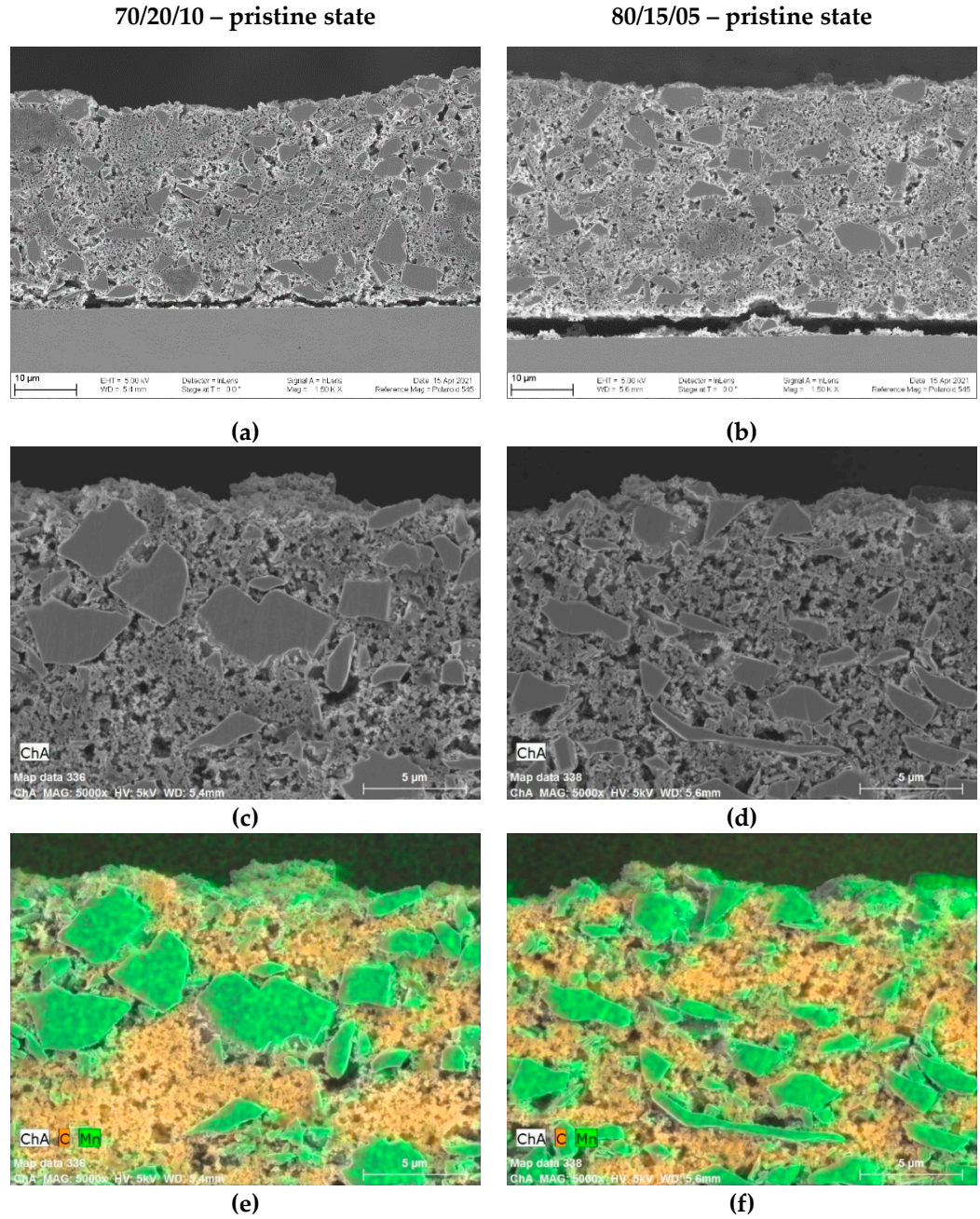*Figure S12: Comparison of the 70/20/10 and 80/15/05 binders in pristine state. For the 80/15/05 coating, smaller distances of the MnO₂ active material particles (coloured green) and a more compact visual impression of the coating could be assumed, which could be referred to the lower CB content and the lower overall passive material (CB + BP) share (20 wt% instead of 30 wt% for the 70/20/10 coating).*
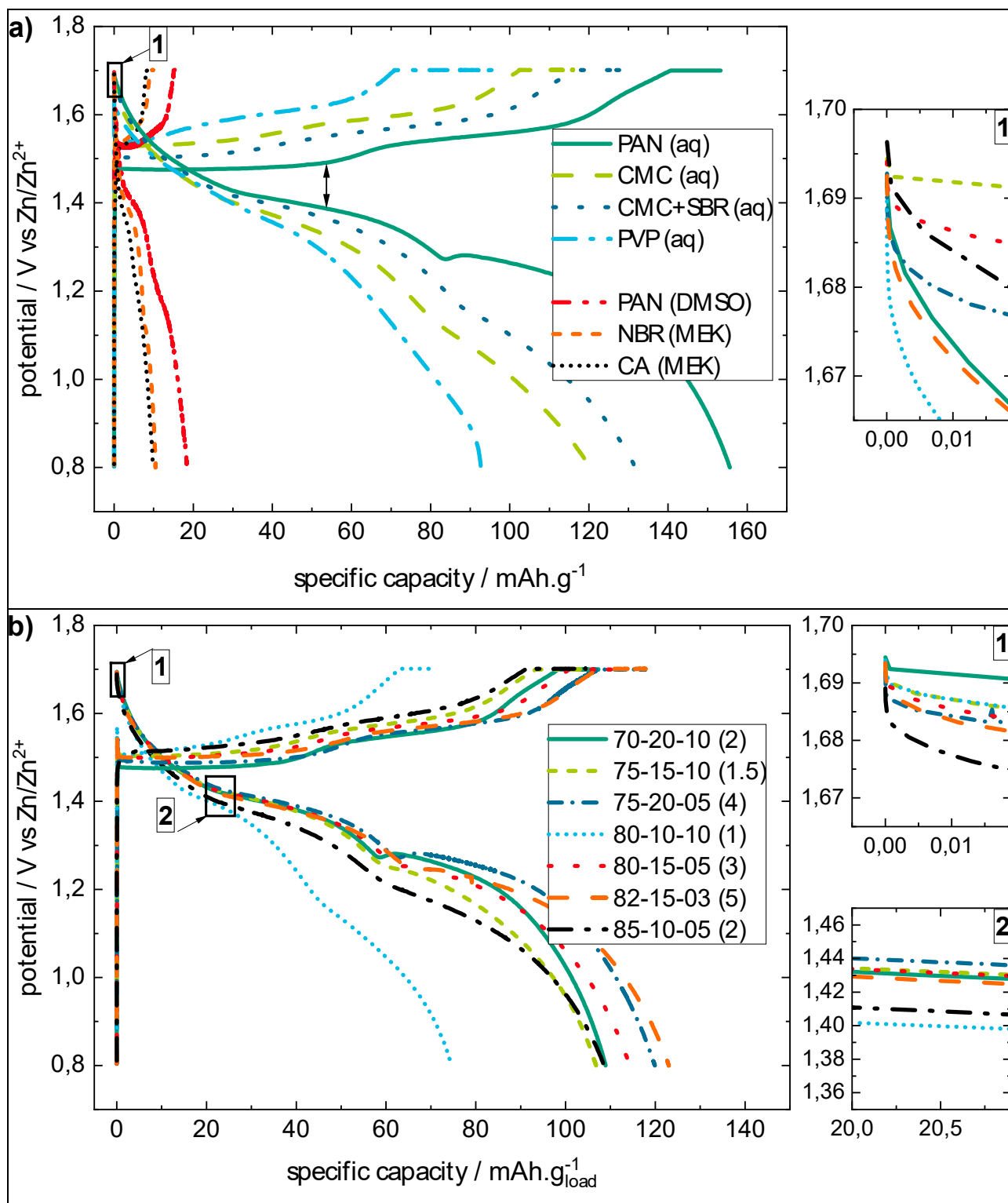
Figure S13: Overview over the charge/discharge curves of the 10th cycle ($80 \, mA.g^{-1}$) of the RCT shown in Figure S4 for the binder variation (a) and mixing variation (b) with insets showing the IR drops directly after the switchover from charge to discharge (marker 1) and the first potential plateau during discharge (marker 2).

(a) Binder variation: The overview of the potential curves reveals differences of the potential plateau hysteresis between the charge/discharge step (s. arrow), which can be related to the inner resistance of the battery cell (including ohmic/charge transfer/diffusion resistance, for example). The initial IR drop after the switchover from charge to discharge (capacity ~0 mAh.g⁻¹) could be an indicator for mainly the electrical (ohmic) resistance of the electrode coating (here: identical electrolyte, cell setup, cell casing, cables, battery tester etc), as the charge transfer/diffusion phenomena only start playing a role in the

course of the discharge. PAN (aq), for example, shows the smallest potential hysteresis between charge/discharge, which can be related to advantages in terms of the inner resistance, whereas CA (MEK) shows a high potential hysteresis indicating a high inner resistance of the battery cell.

(b) Mixing variation: Again, the overview shows differences in terms of the potential hysteresis between the charge/discharge step and the IR-drops after the switchover from charge to discharge, which can reveal insights into the inner resistances of the coatings (here: again, identical electrolyte, cell setup, cell casing, cables, battery tester etc). The coating with the lowest CB/BP-ratio of 1 (s. brackets in the graph legend) and a low CB-content of 10 wt% (coating 80-10-10, AM-CB-BP in wt%) shows the lowest potential plateau level during discharge and discharge capacity, which can be related to the inner resistance of the coating (ohmic/charge transfer/diffusion resistance). In general, there is a trend for coatings with a low CB-content of 10 wt% showing lower potential plateau levels (marker 2) and higher IR-drops after the switchover from charge to discharge (marker 1). In contrast, the higher the CB content of the coating, the higher the potential plateaus (marker 2).

S12. Mechanical stress test (MST): explanation approach for the dissolution phenomena of the aqueous binder-based electrodes in DI-water/electrolyte

The electrolyte solution used in our study was 2 M $ZnSO_4$ + 0.1 M $MnSO_4$. Therefore, only the main component $ZnSO_4$ is considered as a simplification for the following discussion: The solubility of $ZnSO_4$ in water is ~3.5 M [26], which can be determined using the solubility product equation (s. [27], for example). During the solvation of the zinc salt, a solvation shell around the ions is formed by the solvent water (hydration, s. [28]). As the herein used electrolytes are not saturated and have a salt concentration below the solubility of $ZnSO_4$ (here: 2 M), there is still free solvation energy left [28]. Nevertheless, this solvation free energy is reduced by the already dissolved electrolyte salts, compared to the pure DI-water. If the electrode coating comes in contact to either pure DI-water or electrolyte solution as solvents, the binder component as a soluble component could basically dissolve in the solvent. Nevertheless, due to the difference in the solvation free energy of both the solvents, the solvation process is extremely retarded for the electrolyte solution in consequence to the predissolved ions and the reduced solvation free energy, compared to the DI-water. From our point of view, this is the explanation for the observation of the stability of the aqueous binder-based electrodes in electrolyte compared to the instability (dissolution) of these electrodes in pure DI-water.

Literature

1. Chang, H.J.; Rodríguez-Pérez, I.A.; Fayette, M.; Canfield, N.L.; Pan, H.; Choi, D.; Li, X.; Reed, D. Effects of water-based binders on electrochemical performance of manganese dioxide cathode in mild aqueous zinc batteries. *Carbon Energy* **2020**, doi:10.1002/cey2.84.

2. Olbasa, B.W.; Fenta, F.W.; Chiu, S.-F.; Tsai, M.-C.; Huang, C.-J.; Jote, B.A.; Beyene, T.T.; Liao, Y.-F.; Wang, C.-H.; Su, W.-N.; et al. High-Rate and Long-Cycle Stability with a Dendrite-Free Zinc Anode in an Aqueous Zn-Ion Battery Using Concentrated Electrolytes. *ACS Appl. Energy Mater.* **2020**, *3*, 4499–4508, doi:10.1021/acsaem.0c00183.

3. Pan, H.; Ellis, J.; Li, X.; Nie, Z.; Chang, H.J.; Reed, D. Electrolyte Effect on the Electrochemical Performance of Mild Aqueous Zinc-Electrolytic Manganese Dioxide Batteries. *ACS Appl. Mater. Interfaces* **2019**, doi:10.1021/acsami.9b09252.

4. Palaniyandy, N.; Kebede, M.A.; Raju, K.; Ozoemena, K.I.; Le Roux, L.; Mathe, M.K.; Jayaprakasam, R. α-MnO2 nanorod/onion-like carbon composite cathode material for aqueous zinc-ion battery. *Materials Chemistry and Physics* **2019**, *230*, 258–266, doi:10.1016/j.matchemphys.2019.03.069.

5. Hou, Z.; Dong, M.; Xiong, Y.; Zhang, X.; Ao, H.; Liu, M.; Zhu, Y.; Qian, Y. A High-Energy and Long-Life Aqueous Zn/Birnessite Battery via Reversible Water and Zn2+ Coinsertion. *Small* **2020**, e2001228, doi:10.1002/smll.202001228.

6. Guo, X.; Li, J.; Jin, X.; Han, Y.; Lin, Y.; Lei, Z.; Wang, S.; Qin, L.; Jiao, S.; Cao, R. A Hollow-Structured Manganese Oxide Cathode for Stable Zn-MnO2 Batteries. *Nanomaterials* **2018**, *8*, doi:10.3390/nano8050301.

7. Xu, D.; Li, B.; Wei, C.; He, Y.-B.; Du, H.; Chu, X.; Qin, X.; Yang, Q.-H.; Kang, F. Preparation and Characterization of MnO2/acid-treated CNT Nanocomposites for Energy Storage with Zinc Ions. *Electrochimica Acta* **2014**, *133*, 254–261, doi:10.1016/j.electacta.2014.04.001.

8. Bischoff, C.; Fitz, O.; Schiller, C.; Gentischer, H.; Biro, D.; Henning, H.-M. Investigating the Impact of Particle Size on the Performance and Internal Resistance of Aqueous Zinc Ion Batteries with a Manganese Sesquioxide Cathode. *MDPI Batteries* **2018**, *4*, 44, doi:10.3390/batteries4030044.

9. Chamoun, M.; Brant, W.R.; Tai, C.-W.; Karlsson, G.; Noréus, D. Rechargeability of aqueous sulfate Zn/MnO 2 batteries enhanced by accessible Mn 2+ ions. *Energy Storage Materials* **2018**, *15*, 351–360, doi:10.1016/j.ensm.2018.06.019.

10. Zhang, N.; Cheng, F.; Liu, J.; Wang, L.; Long, X.; Liu, X.; Li, F.; Chen, J. Rechargeable aqueous zinc-manganese dioxide batteries with high energy and power densities. *Nat. Commun.* **2017**, *8*, 405, doi:10.1038/s41467-017-00467-x.

11. Jiang, B.; Xu, C.; Wu, C.; Dong, L.; Li, J.; Kang, F. Manganese Sesquioxide as Cathode Material for Multivalent Zinc Ion Battery with High Capacity and Long Cycle Life. *Electrochimica Acta* **2017**, *229*, 422–428, doi:10.1016/j.electacta.2017.01.163.

12. Pan, H.; Shao, Y.; Yan, P.; Cheng, Y.; Han, K.S.; Nie, Z.; Wang, C.; Yang, J.; Li, X.; Bhattacharya, P.; et al. Reversible aqueous zinc/manganese oxide energy storage from conversion reactions. *Nat. Energy* **2016**, *1*, 16039, doi:10.1038/nenergy.2016.39.

13. Islam, S.; Alfaruqi, M.H.; Mathew, V.; Song, J.; Kim, S.; Kim, S.; Jo, J.; Baboo, J.P.; Pham, D.T.; Putro, D.Y.; et al. Facile synthesis and the exploration of the zinc storage mechanism of β-MnO2 nanorods with exposed (101) planes as a novel cathode material for high performance eco-friendly zinc-ion batteries. *J. Mater. Chem. A* **2017**, *5*, 23299–23309, doi:10.1039/C7TA07170A.

14. Poyraz, A.S.; Laughlin, J.; Zec, Z. Improving the cycle life of cryptomelane type manganese dioxides in aqueous rechargeable zinc ion batteries: The effect of electrolyte concentration. *Electrochimica Acta* **2019**, *305*, 423–432, doi:10.1016/j.electacta.2019.03.093.

15. Huang, J.; Wang, Z.; Hou, M.; Dong, X.; Liu, Y.; Wang, Y.; Xia, Y. Polyaniline-intercalated manganese dioxide nanolayers as a high-performance cathode material for an aqueous zinc-ion battery. *Nat. Commun.* **2018**, *9*, 2906, doi:10.1038/s41467-018-04949-4.

16. Zeng, X.; Liu, J.; Mao, J.; Hao, J.; Wang, Z.; Zhou, S.; Ling, C.D.; Guo, Z. Toward a Reversible Mn4+/Mn2+ Redox Reaction and Dendrite‐Free Zn Anode in Near‐Neutral Aqueous Zn/MnO 2 Batteries via Salt Anion Chemistry. *Adv. Energy Mater.* **2020**, *10*, 1904163, doi:10.1002/aenm.201904163.

17. Guo, X.; Zhou, J.; Bai, C.; Li, X.; Fang, G.; Liang, S. Zn/MnO2 battery chemistry with dissolution-deposition mechanism. *Materials Today Energy* **2020**, *16*, 100396, doi:10.1016/j.mtener.2020.100396.

18. Sun, W.; Wang, F.; Hou, S.; Yang, C.; Fan, X.; Ma, Z.; Gao, T.; Han, F.; Hu, R.; Zhu, M.; et al. Zn/MnO2 Battery Chemistry With H+ and Zn2+ Coinsertion. *J. Am. Chem. Soc.* **2017**, *139*, 9775–9778, doi:10.1021/jacs.7b04471.

19. Xu, C.; Li, B.; Du, H.; Kang, F. Energetic zinc ion chemistry: the rechargeable zinc ion battery. *Angew. Chem. Int. Ed Engl.* **2012**, *51*, 933–935, doi:10.1002/anie.201106307.

20. Lee, B.; Yoon, C.S.; Lee, H.R.; Chung, K.Y.; Cho, B.W.; Oh, S.H. Electrochemically-induced reversible transition from the tunneled to layered polymorphs of manganese dioxide. *Sci. Rep.* **2014**, *4*, 6066, doi:10.1038/srep06066.

21. Lee, B.; Lee, H.R.; Kim, H.; Chung, K.Y.; Cho, B.W.; Oh, S.H. Elucidating the intercalation mechanism of zinc ions into α-MnO2 for rechargeable zinc batteries. *Chem. Commun. (Camb)* **2015**, *51*, 9265–9268, doi:10.1039/C5CC02585K.

22. Wu, B.; Zhang, G.; Yan, M.; Xiong, T.; He, P.; He, L.; Xu, X.; Mai, L. Graphene Scroll-Coated α-MnO2 Nanowires as High-Performance Cathode Materials for Aqueous Zn-Ion Battery. *Small* **2018**, *14*, e1703850, doi:10.1002/smll.201703850.

23. Alfaruqi, M.H.; Mathew, V.; Gim, J.; Kim, S.; Song, J.; Baboo, J.P.; Choi, S.H.; Kim, J. Electrochemically Induced Structural Transformation in a γ-MnO2 Cathode of a High Capacity Zinc-Ion Battery System. *Chem. Mater.* **2015**, *27*, 3609–3620, doi:10.1021/cm504717p.

24. Alfaruqi, M.H.; Gim, J.; Kim, S.; Song, J.; Pham, D.T.; Jo, J.; Xiu, Z.; Mathew, V.; Kim, J. A layered δ-MnO2 nanoflake cathode with high zinc-storage capacities for eco-friendly battery applications. *Electrochemistry Communications* **2015**, *60*, 121–125, doi:10.1016/j.elecom.2015.08.019.

25. Han, S.-D.; Kim, S.; Li, D.; Petkov, V.; Yoo, H.D.; Phillips, P.J.; Wang, H.; Kim, J.J.; More, K.L.; Key, B.; et al. Mechanism of Zn Insertion into Nanostructured δ-MnO2 : A Nonaqueous Rechargeable Zn Metal Battery. *Chem. Mater.* **2017**, *29*, 4874–4884, doi:10.1021/acs.chemmater.7b00852.

26. *CRC Handbook of Chemistry and Physics: A ready-reference book of chemical and physical data;* Haynes, W.M., Ed., 97th edition; CRC Press: Boca Raton, London, New York, 2017, ISBN 9781498754286.

27. Oxtoby, D.W.; Gillis, H.P.; Campion, A. *Principles of modern chemistry*; Recording for the Blind & Dyslexic: Princeton, N.J., 2007, ISBN 978-0-534-49366-0.

28. Bard, A.J.; Inzelt, G.; Scholz, F. *Electrochemical Dictionary*, 2nd ed. 2013; Springer: Berlin, Heidelberg, 2012, ISBN 9783642295515.